INTERNATIONAL JOURNAL FOR NUMERICAL METHODS IN FLUIDS, VOL. 10, 637–649 (1990)

SIMULATION OF PLANAR CONVERGING FLOW OF A LEONOV VISCOELASTIC FLUID

HSIENG-CHENG TSENG

Department of Chemical Engineering, National Taiwan Institute of Technology, Taipei 10772, R.O.C.,

AND

GWO-GENG LIN

Department of Chemical Engineering, Tamkang University, Tamsui, Taiwan 25137, R.O.C.

SUMMARY

An efficient finite element algorithm is presented to simulate the planar converging flow for the viscoelastic fluid of the Leonov model. The governing equation set, composed of the continuity, momentum and constitutive equations for the Leonov fluid flow, is conveniently decoupled and a two-stage cyclic iteration technique is employed to solve the velocity and elastic strain fields separately. Artificial viscosity terms are imposed on the momentum equations to relax the elastic force and data smoothing is performed on the iterative calculations for velocities to further stabilize the numerical computations. The calculated stresses agree qualitatively with the experimental measurements and other numerically simulated results available in the literature. Computations were successful to moderately high values of Deborah number of about 27·5.

KEY WORDS Viscoelastic flow Planar converging flow Leonov model Artificial viscosity Data smoothing

INTRODUCTION

Numerical simulation of viscoelastic fluid flows accompanied by the so-called high-Deborah-number problem has been an active research area of non-Newtonian fluid mechanics in the last decade.[1–7] Yeh[8] systematically categorized the possible causes for the numerical difficulties into five classes in a contraction flow simulation and attempted to improve the numerical scheme by trying different techniques, but the calculations were still limited to the critical Deborah number of unity. A good review of works related to the numerical and experimental study of contraction flow was given by White *et al.*[9] They indicated that for a number of viscoelastic models, numerical calculations usually failed to converge at relatively low shear rates (with Deborah number of the order of unity). Crochet *et al.* stated the same conclusions for the calculations of different viscoelastic flow situations in their book.[10]

Considerable progress has been made, however, through the deeper mathematical understanding of the set of equations involved. Beris *et al.* have demonstrated the formation of stress boundary layers that cause the breakdown of numerical solutions at high Deborah number in both perturbation analysis[11] and spectral/finite element calculations[12] for the viscoelastic flow between two eccentric rotating cylinders. Recently, King *et al.*[13] used the reconstructed explicitly elliptic momentum equation to simulate upper convected Maxwell and modified upper convected Maxwell fluid flow in singular geometries and reported that the calculations were limited at high

0271–2091/90/060637–13$06.50

Received March 1989
Revised June 1989

values of Deborah number. Debbaut *et al.*[14] developed a new mixed algorithm simultaneously introducing both multiple bilinear stress sub-elements and the streamline-upwinding technique and obtained solutions at very high Deborah number, but they pointed out that such a method is very expensive in view of the large frontal width caused by the stress sub-elements. It is worth noting that progress up to now has been restricted to the most often used Maxwellian-type rheological models.

In order to direct the study of non-Newtonian fluid mechanics towards 'realistic' polymer flow simulation, it is essential to select proper constitutive equations beyond those of the simple Maxwellian type and to compare the simulated results with experimental measurements. The Leonov model[15,16] has been employed extensively by the research group of CIMP (Cornell Injection Molding Project, Cornell University, Ithaca, NY) to study the viscoelastic flow of polymeric material in the injection moulding process since 1978. They have concluded that the Leonov model can be satisfactorily applied to predict the different flow situations[17–19] where the viscoelasticity of the polymeric material is known to be significant. From the numerical point of view, the potential advantages of using the Leonov model are that the material parameters can be easily found from simple rheological experiments and that the resulting equations are readily amenable to numerical implementation. Upadhyay and Isayev[20] have developed a numerical scheme to simulate the two-dimensional flow of a Leonov fluid, where the streamwise integration procedure[21] was used to integrate the constitutive equations. Artificial viscosity terms were also imposed on the momentum equations to relax the elastic force, thus stabilizing the numerical calculations. The streamwise integration has some drawbacks[22,23] which motivate this study to develop a different approach to solve the Leonov constitutive equations.

It was generally agreed that the numerical difficulties of the simulation of viscoelastic flow were divided into three parts, namely (1) the integration of stresses, (2) the coupling between stresses and velocities and (3) the iterative scheme.[24] With regard to the integration of the Leonov constitutive equations, which comprise a non-linear hyperbolic system of partial differential equations with an equality constraint, an effective finite element scheme has been successfully developed in the preliminary part of this study.[25] In addition the deviatoric stress for the Leonov model is skilfully decomposed into viscous and elastic parts. The constitutive equation, which is then represented in terms of the elastic strain (**C**), can be conveniently decoupled from the equations of motion if a two-stage cyclic iteration technique[20] is employed to solve the velocity and elastic strain fields separately. In this paper such an iterative scheme has been implemented with an efficient finite element algorithm to simulate the planar converging flow for a Leonov fluid and has proved to resolve the difficulties (2) and (3) mentioned above.

THEORETICAL MODELLING FOR THE CONVERGING FLOW

Basic equations

For a planar, inertia-free, incompressible Leonov fluid flow with no body forces, the governing equations reduce to

$$\nabla \cdot \mathbf{v} = 0, \tag{1}$$

$$-\nabla p + \eta_0 s \nabla^2 \mathbf{v} + \sum_{k=1}^{N} \frac{\eta_k}{\theta_k} \nabla \cdot \mathbf{C}^k = \mathbf{0}, \tag{2}$$

$$\frac{\partial \mathbf{C}^k}{\partial t} + \mathbf{v} \cdot \nabla \mathbf{C}^k - \nabla \mathbf{v}^{\mathrm{T}} \cdot \mathbf{C}^k - \mathbf{C}^k \cdot \nabla \mathbf{v} + \frac{1}{2\theta_k} (\mathbf{C}^k \cdot \mathbf{C}^k - \mathbf{I}) = \mathbf{0}, \tag{3}$$

where $\mathbf{v}$ is the velocity vector, p is the indeterminate pressure, $\mathbf{I}$ is the unit tensor and $\mathbf{C}^k$ is the elastic strain tensor for the kth mode of the Leonov model, with η_k and θ_k being the corresponding shear viscosity and relaxation time respectively. η_0 is the zero-shear-rate viscosity and s is a rheological parameter lying between zero and one. η_0 is related to s and η_k as[17]

$$\eta_0 = \sum_{k=1}^{N} \frac{\eta_k}{1-s}.$$

For two-dimensional problems the components for $\mathbf{C}^k$ are

$$\mathbf{C}^k = \begin{bmatrix} C_{11}^k & C_{12}^k & 0 \\ C_{12}^k & C_{22}^k & 0 \\ 0 & 0 & 1 \end{bmatrix}.$$

The simultaneous equations (1)–(3) can be decoupled and solved by a two-stage cyclic iteration technique. First, for an initial guess of the velocity field $\mathbf{v}$, the tensor equation (3) can be integrated independently by using a Galerkin finite element algorithm (see Reference 25 for details). With the elastic strain tensor $\mathbf{C}^k$ being solved, the velocity and pressure can then be solved from equations (1) and (2). This is equivalent to solving purely viscous flow with a body force. The whole process can be viewed as a relaxation from the approximate velocity and stress fields to a steady state where both the velocity and stresses are compatible.

Finite element formulation

The artificial viscosity method was applied to relax the elastic force in the momentum equations.[20] The momentum and continuity equations in component form for rectangular Cartesian co-ordinates are then given by

$$-(\eta_0 s+\omega)\left(\frac{\partial^2 u}{\partial x^2}+\frac{\partial^2 u}{\partial y^2}\right)_{m+1} + \frac{\partial p}{\partial x} = -\omega\left(\frac{\partial^2 u}{\partial x^2}+\frac{\partial^2 u}{\partial y^2}\right)_m + \sum_{k=1}^{N}\frac{\eta_k}{\theta_k}\left(\frac{\partial C_{11}^k}{\partial x}+\frac{\partial C_{12}^k}{\partial y}\right), \quad (4)$$

$$-(\eta_0 s+\omega)\left(\frac{\partial^2 v}{\partial x^2}+\frac{\partial^2 v}{\partial y^2}\right)_{m+1} + \frac{\partial p}{\partial y} = -\omega\left(\frac{\partial^2 v}{\partial x^2}+\frac{\partial^2 v}{\partial y^2}\right)_m + \sum_{k=1}^{N}\frac{\eta_k}{\theta_k}\left(\frac{\partial C_{12}^k}{\partial x}+\frac{\partial C_{22}^k}{\partial y}\right), \quad (5)$$

$$\frac{\partial u}{\partial x}+\frac{\partial v}{\partial y}=0, \quad (6)$$

where u, v are the x, y components of the velocity vector and ω is the artificial viscosity which is prescribed to be very close to η_0 from numerical experience. The subscripts m and $m+1$ indicate the mth and $(m+1)$th iteration respectively.

The unknown variables over every discretized element are approximated as

$$u \approx \tilde{u} = \sum_i \psi_i \tilde{u}_i, \qquad v \approx \tilde{v} = \sum_i \psi_i \tilde{v}_i, \qquad p \approx \tilde{p} = \sum_i \phi_i \tilde{p}_i.$$

The Galerkin method is applied to equations (4)–(6) with the velocity interpolation functions ψ_i being used as weighting functions for the equations of motion, (4) and (5), and the pressure interpolation functions ϕ_i being used as weighting functions for the continuity equation (6).

That is,

$$\int_A [\text{equation (4)}]\,\psi_i\,\mathrm{d}A = 0, \tag{7}$$

$$\int_A [\text{equation (5)}]\,\psi_i\,\mathrm{d}A = 0, \tag{8}$$

$$\int_A [\text{equation (6)}]\,\phi_i\,\mathrm{d}A = 0, \tag{9}$$

Equations (7)–(9) result in a system of algebraic equations for the nodal unknowns $\{\tilde{u}_i\}$, $\{\tilde{v}_i\}$ and $\{\tilde{p}_i\}$ as follows:

$$\begin{bmatrix} [k_{11}] & [0] & [k_{13}] \\ [0] & [k_{22}] & [k_{23}] \\ [k_{13}] & [k_{23}] & [0] \end{bmatrix} \begin{Bmatrix} \{\tilde{u}_i\} \\ \{\tilde{v}_i\} \\ \{\tilde{p}_i\} \end{Bmatrix} = \begin{Bmatrix} \{r_1\} \\ \{r_2\} \\ \{0\} \end{Bmatrix}, \tag{10}$$

where

$$[k_{11}] = \int_A (\eta_0 s + \omega)\left(\left\{\frac{\partial \psi}{\partial x}\right\}\left\{\frac{\partial \psi}{\partial x}\right\}^{\mathrm{T}} + \left\{\frac{\partial \psi}{\partial y}\right\}\left\{\frac{\partial \psi}{\partial y}\right\}^{\mathrm{T}} \right) \mathrm{d}A,$$

$$[k_{13}] = -\int_A \left\{\frac{\partial \psi}{\partial x}\right\}\{\phi\}^{\mathrm{T}}\,\mathrm{d}A,$$

$$[k_{22}] = [k_{11}],$$

$$[k_{23}] = -\int_A \left\{\frac{\partial \psi}{\partial y}\right\}\{\phi\}^{\mathrm{T}}\,\mathrm{d}A,$$

$$\{r_1\} = \int_A \{\psi\} f_x\,\mathrm{d}A + \left[\oint (\eta_0 s + \omega)\{\psi\} t_x\,\mathrm{d}S\right]_{m+1} - \left[\oint \omega\{\psi\}\,\hat{t}_x\,\mathrm{d}S\right]_m + \left[\int_A \omega\left(\left\{\frac{\partial \psi}{\partial x}\right\}\frac{\partial \tilde{u}}{\partial x} + \left\{\frac{\partial \psi}{\partial y}\right\}\frac{\partial \tilde{u}}{\partial y}\right)\mathrm{d}A\right]_m,$$

$$\{r_2\} = \int_A \{\psi\} f_y\,\mathrm{d}A + \left[\oint (\eta_0 s + \omega)\{\psi\} t_y\,\mathrm{d}S\right]_{m+1} - \left[\oint \omega\{\psi\}\,\hat{t}_y\,\mathrm{d}S\right]_m + \left[\int_A \omega\left(\left\{\frac{\partial \psi}{\partial x}\right\}\frac{\partial \tilde{v}}{\partial x} + \left\{\frac{\partial \psi}{\partial y}\right\}\frac{\partial \tilde{v}}{\partial y}\right)\mathrm{d}A\right]_m,$$

$$f_x = \sum_{k=1}^{N} \frac{\eta_k}{\theta_k}\left(\frac{\partial C_{11}^k}{\partial x} + \frac{\partial C_{12}^k}{\partial y}\right),$$

$$f_y = \sum_{k=1}^{N} \frac{\eta_k}{\theta_k}\left(\frac{\partial C_{12}^k}{\partial x} + \frac{\partial C_{22}^k}{\partial y}\right),$$

$$t_x = \frac{\partial u}{\partial x} n_x + \frac{\partial u}{\partial y} n_y - p n_x,$$

$$t_y = \frac{\partial v}{\partial x} n_x + \frac{\partial v}{\partial y} n_y - p n_y,$$

$$\hat{t}_x = \frac{\partial u}{\partial x} n_x + \frac{\partial u}{\partial y} n_y,$$

$$\hat{t}_y = \frac{\partial v}{\partial x} n_x + \frac{\partial v}{\partial y} n_y.$$

These area integrals over each element were evaluated by using a three-point Gaussian quadrature. A global stiffness matrix is obtained by assembling the above matrix $[K]$ from each element. The matrix is symmetric, banded and remains unchanged during the iterative process. The shape of the elements is taken to be rectangular, with the velocity being interpolated quadratically and the pressure linearly, as a common procedure. The values of $\mathbf{C}^k$ are computed at the Gauss points interpolated quadratically from the nodal values which were solved independently from the previously iterated velocity field via another FEM scheme.[25] The following data-smoothing technique[10] was used in the iterative calculations for velocity to stabilize the numerical computations:

$$(1-\beta_x)\mathbf{X}_{m+1} + \beta_x \mathbf{X}_m \rightarrow \mathbf{X}_{m+1}, \quad \beta_x \in [0, 1],$$

where $\mathbf{X}$ denotes the velocity vector and β_x is set to 0·5. The subscripts m and $m+1$ indicate the mth and $(m+1)$th iteration respectively.

Sample problem

Han and Drexler[26] have presented some measurements of stresses for polystyrene (Dow Chemical 686) melt flowing through a 60° converging slit die. The flow birefringence technique was used to measure stress patterns. The narrow slit had a cross-section of $1{\cdot}99 \times 0{\cdot}199$ cm^2. The experiment was carried out at 200 °C for a flow rate of 5·36 cm^3 min^{-1}, which corresponds to an average velocity U_{avg} in the narrow slit of 0·2256 cm s^{-1}. For the purpose of comparison, the planar converging flow system illustrated in Figure 1 was numerically simulated to test the FEM algorithm presented. The following values of the rheological parameters for the two-mode Leonov model fitted from the steady state shear viscosity were used in the numerical computations:[27]

$$s = 0{\cdot}0041, \ \theta_1 = 8{\cdot}43 \times 10^{-1} \text{ s}, \ \eta_1 = 2{\cdot}28 \times 10^4 \text{ Pa s}, \ \theta_2 = 1{\cdot}56 \times 10^{-2} \text{ s}, \ \eta_2 = 8{\cdot}85 \times 10^2 \text{ Pa s}.$$

The Deborah number is defined as[20]

$$De = \tilde{\theta} \frac{3U_{avg}}{B},$$

where B is the half-gap thickness of the narrow slit and $\tilde{\theta}$ is the characteristic relaxation time of the material defined as

$$\tilde{\theta} = \frac{\sum_{k=1}^{N} \eta_k \theta_k}{\eta_0}.$$

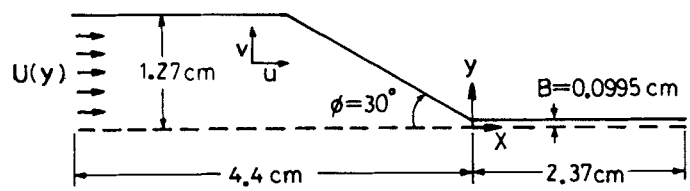

Figure 1. Schematic diagram of the planar converging flow

For the polymer considered above, the characteristic time $\tilde{\theta}$ is 0·81 s and *De* is about 5·5 for this sample problem.

The no-slip condition $\mathbf{v}=\mathbf{0}$ is imposed on solid walls and the symmetry condition is imposed along the central axis. Fully developed velocity profiles are assumed at both entry and exit, while fully developed elastic strain ($\mathbf{C}^k$) profiles are assumed at entry but not at exit.

RESULTS AND DISCUSSION

Four cases based on different conditions, as shown in Table I, have been considered in our finite element calculations. The meshes A and B are very similar with only slight changes near the re-entrant corner as shown in Figure 2. The numbers of elements are 150 and 175 and the total numbers of nodes are 671 and 781 for meshes A and B respectively. Simulated contour plots of the stresses for the three sample calculations RUN1, RUN2 and RUN3 together with the corresponding experimental data of Han and Drexler[26] are shown in Figures 3–9 for comparison. It can be seen from Figures 3 and 4 that the use of data smoothing in the iterative velocity calculations is effective for the improvement of numerical stability. The effect of mesh refinement on the

Table I. Sample calculations based on different meshes and the use of velocity smoothing

Sample run	Mesh	With data smoothing in velocity calculations	*De*
RUN1	A	No	5·5
RUN2	A	Yes	5·5
RUN3	B	Yes	5·5
RUN4	B	Yes	27·5

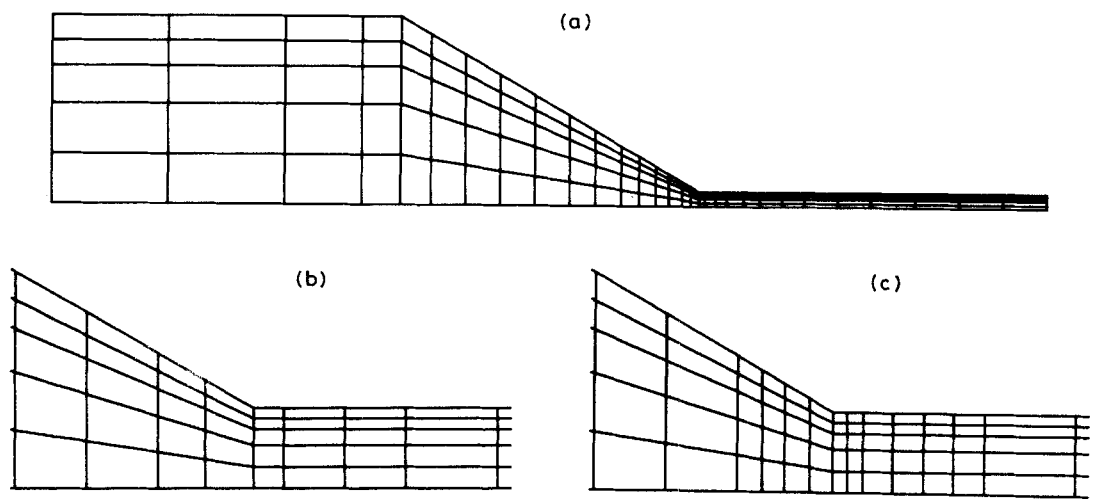

Figure 2. (a) Figure element mesh A for the whole flow domain under analysis. (b) Finite element mesh A near the entrance to the slit. (c) Finite element mesh B near the entrance to the slit; elsewhere mesh B and mesh A are identical

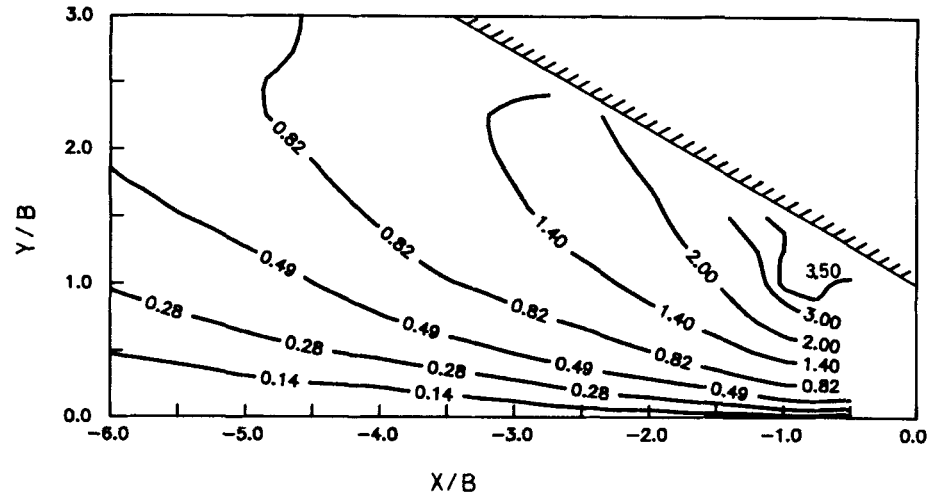

Figure 3. Contours of the calculated shear stress ($\tau_{xy} \times 10^{-4}$ Pa) for RUN1 near the entrance to the slit

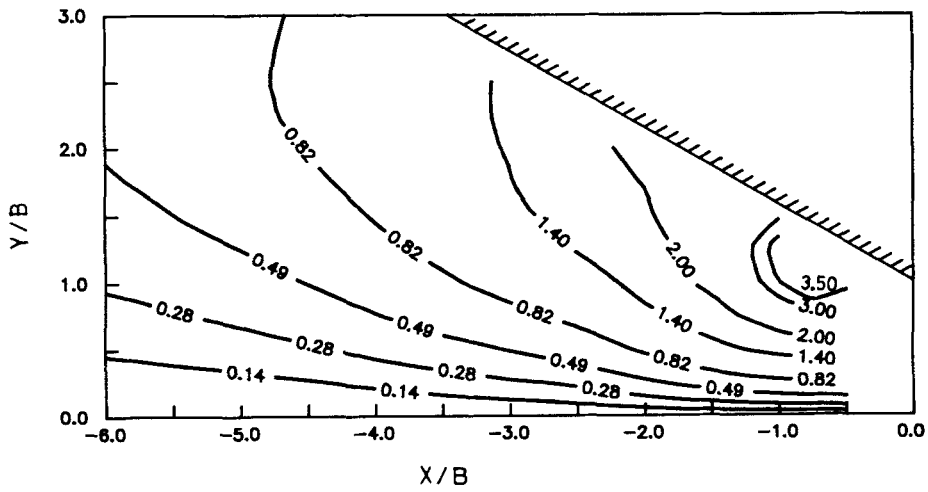

Figure 4. Contours of the calculated shear stress ($\tau_{xy} \times 10^{-4}$ Pa) for RUN2 near the entrance to the slit

calculation can be observed by comparison of Figures 4 and 5 and of Figures 6 and 7. The difference in the contour lines of shear stress shown in Figures 4 and 5 is quite small. Figures 6 and 7 suggest that the oscillations of the contour lines for the first normal stress difference N_1 (i.e. $\tau_{xx} - \tau_{yy}$) with mesh A are due to the discretization error resulting from too coarse a mesh, since such oscillations are not seen in the case of the finer mesh B. From our numerical experience, the number of iterations required for convergence is larger and the critical Deborah number up to which the convergent solutions can be obtained is lower for computations without velocity smoothing than for those with it. Therefore both the velocity smoothing and the finer mesh B are essential for the numerical simulation presented in this paper.

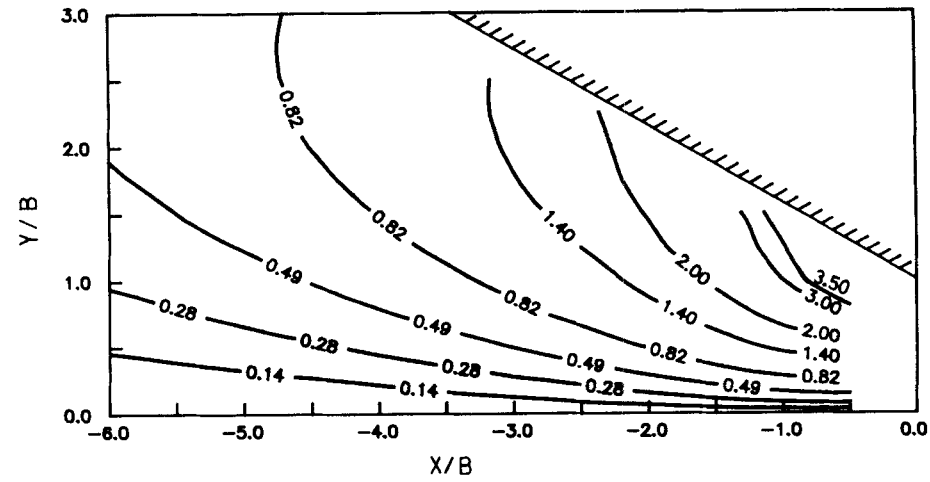

Figure 5. Contours of the calculated shear stress ($\tau_{xy} \times 10^{-4}$ Pa) for RUN3 near the entrance to the slit

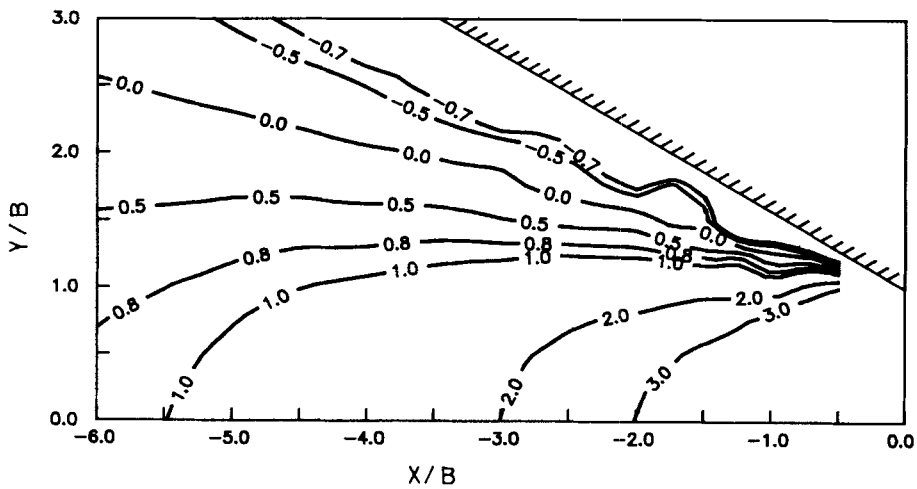

Figure 6. Contours of the calculated first normal stress difference ($N_1 \times 10^{-4}$ Pa) for RUN2 near the entrance to the slit

The present results agree well quantitatively with those of Upadhyay[27] (not shown here) where the constitutive equations were integrated along the streamline. It is worth noting that the simulated results and the experimental measurements are in agreement only qualitatively (cf. Figures 5 and 8 and Figures 7 and 9). One conceivable explanation of the discrepancy between the numerical modelling and experiments is that the rheological data are not sufficiently accurate for characterization of the material.[27] Another source of the discrepancy may be that the entry and exit channels used in the experiment of Han and Drexler[26] were not long enough, so that the assumption of fully developed flow conditions in our theoretical analysis was not exactly compatible.

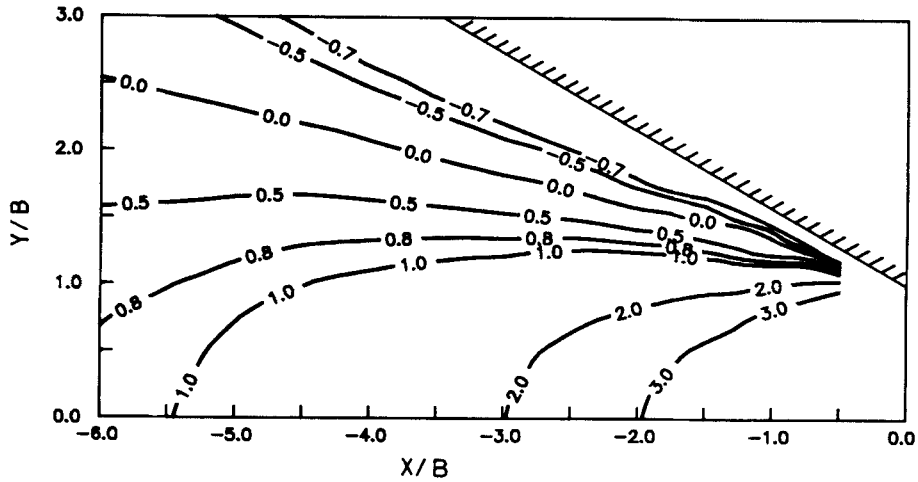

Figure 7. Contours of the calculated first normal stress difference ($N_1 \times 10^{-4}$ Pa) for RUN3 near the entrance to the slit

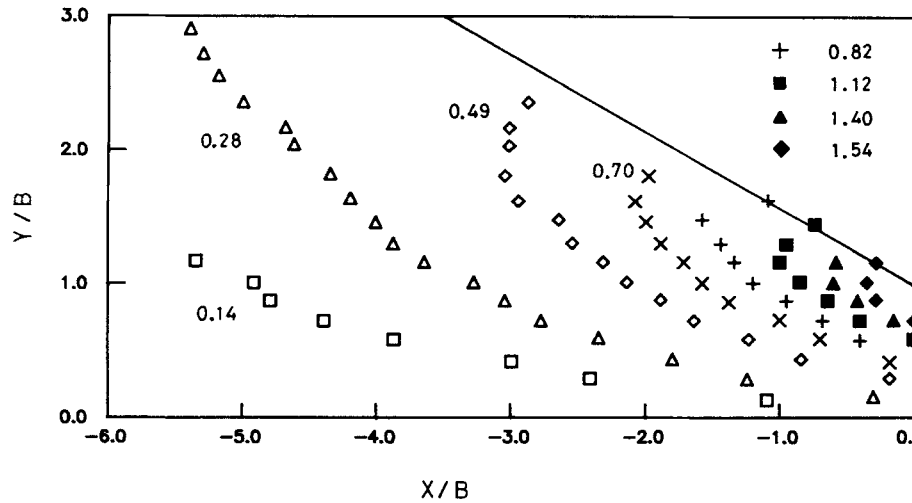

Figure 8. Contours of the measured shear stress ($\tau_{xy} \times 10^{-4}$ Pa) near the entrance to the slit of Han and Drexler[26]

Computations were successful for Deborah number up to 27·5, attained by increasing the flow rate while keeping the rheological parameters unchanged. Figure 10 shows the contour lines for the calculated first normal stress difference for RUN4 just before the divergence of computation. It can be seen that fluctuations of the contour lines appear near the solid wall where large stress gradients were generated.

To avoid redundancy, the following discussion will be based on the simulated results for RUN3. Figure 11 shows variations of both the first normal stress difference and its viscous part D ($=4\,\eta_0 s\,\partial u/\partial x$) along the centreline. The velocity gradient $\partial u/\partial x$ in the viscous part D of the first normal stress difference indicates the extent of acceleration of the fluid element along the flow direction X. These two nearly synchronous curves in Figure 11 manifestly justify the significance

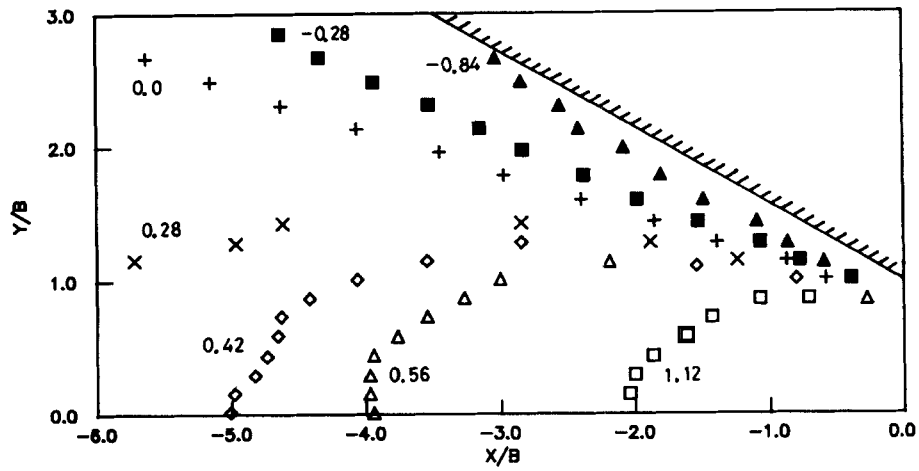

Figure 9. Contours of the measured first normal stress difference ($N_1 \times 10^{-4}$ Pa) near the entrance to the slit of Han and Drexler[26]

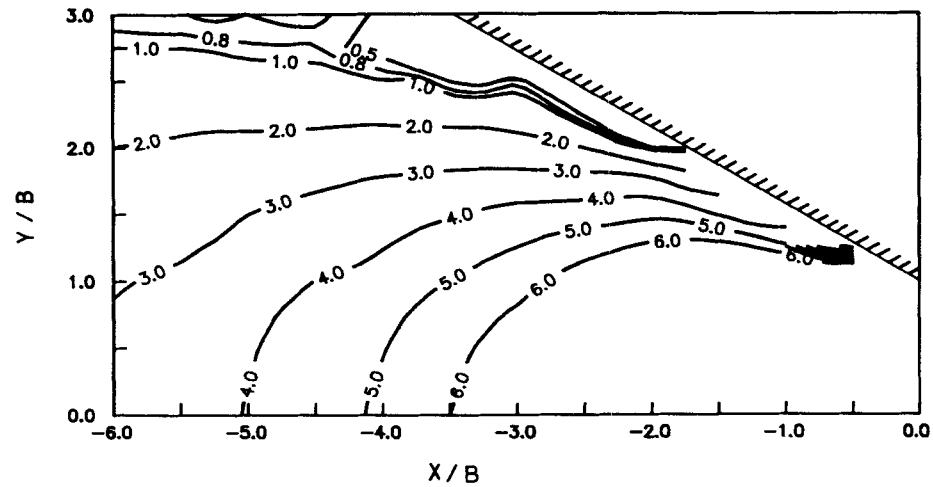

Figure 10. Contours of the calculated first normal stress difference ($N_1 \times 10^{-4}$ Pa) for RUN4 near the entrance to the slit

of the elongational flow with respect to the elastic force generated in the converging viscoelastic flow, although the viscous contribution is two orders of magnitude smaller than that of the total first normal stress difference.

Variations of the normal stress and isotropic pressure along the converging wall are shown in Figure 12(a). The profiles for both normal stress and pressure exhibit a tendency to increase near the inlet to the small slit, as was observed experimentally by Han[28] for polyethylene and polypropylene melts flowing in a 30° converging channel. Figure 12(b) shows a slight overshoot in the axial velocity profile along the centreline, which has been seen for most viscoelastic flows.

Overall, the physical phenomena observed in Han and Drexler's experiment[26] are well described by the model simulation of the present study, but quantitative comparison is inconclusive. As mentioned above, this may require well controlled experiments (e.g. the same

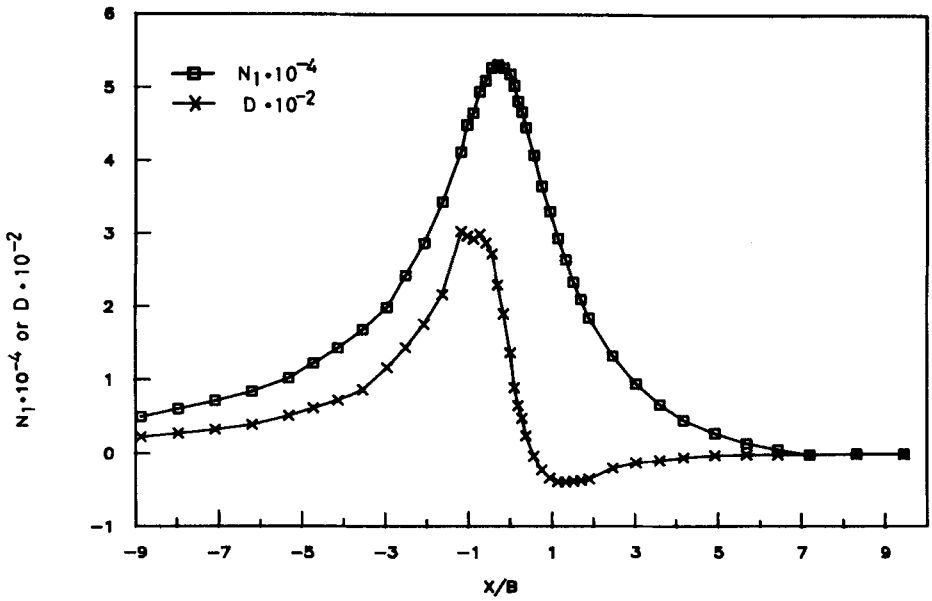

Figure 11. First normal stress difference ($N_1 \times 10^{-4}$ Pa) and its viscous part ($D \times 10^{-2}$ Pa; $D = 4\eta_0 s\, \partial u/\partial x$) along the centreline. Symbols: grid points

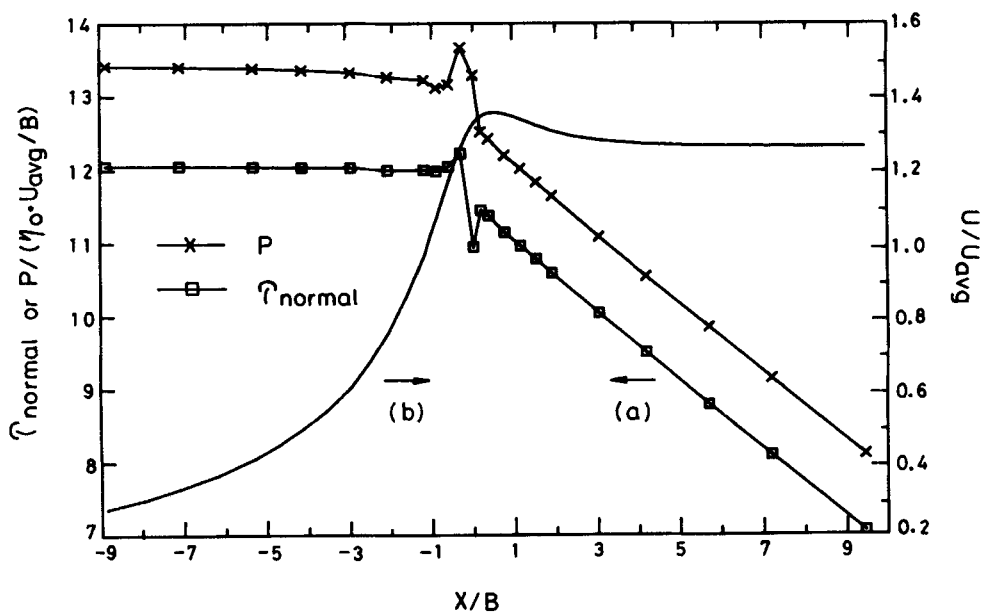

Figure 12. (a) Normal stress τ_{normal} and isotropic pressure p along the wall. (b) Axial velocity profile along the centreline. Symbols: grid points

boundary conditions for both experimental investigation and theoretical modelling) and good rheological characterization of the polymeric material.

CONCLUSIONS

We have presented an efficient finite element technique with a two-stage cyclic iterative scheme by use of which a planar converging flow of a polymeric material is numerically simulated with the Leonov rheological model. Artificial viscosity terms were imposed on the momentum equations to relax the elastic force and data smoothing was performed on the iterative calculations for velocities to further stabilize the numerical computations. The calculated stresses agree qualitatively with the experimental measurements and other numerically simulated results available in the literature. Computations with mesh refinement were successful to moderately high values of Deborah number of about 27·5. It will be useful in the future to generalize this method to simulations with other viscoelastic models of differential type.

ACKNOWLEDGEMENTS

This work has been supported by the National Science Council, R.O.C., under Grant No. NSC77-0405-E011-04. The valuable comments on the Leonov rheological model given by Dr. C. A. Hieber of Cornell University are also gratefully acknowledged.

REFERENCES

1. M. J. Crochet and M. Bezy, 'Numerical solution for the flow of viscoelastic fluids', *J. Non-Newtonian Fluid Mech.*, **5**, 201–218 (1979).
2. M. G. N. Perera and K. Strauss, 'Direct numerical solutions of the equations for viscoelastic fluid flow', *J. Non-Newtonian Fluid Mech.*, **5**, 269–283 (1979).
3. M. J. Crochet and R. Keunings, 'Die swell of a Maxwell fluid: numerical prediction', *J. Non-Newtonian Fluid Mech.*, **7**, 199–212 (1980).
4. C. J. Coleman, 'A finite element routine for analyzing non-Newtonian flows. Part I: Basic method and preliminary results', *J. Non-Newtonian Fluid Mech.*, **7**, 289–301 (1980).
5. E. Mitsoulis, 'Finite element analysis of two-dimensional polymer melt flows', *Ph.D. Thesis*, McMaster University, Hamilton, Ontario 1984.
6. R. Keunings, 'On the high Weissenberg number problem', *J. Non-Newtonian Fluid Mech.*, **20**, 209–226 (1986)
7. G. G. Lipscomb, R. Keunings and M. M. Denn, 'Implications of boundary singularities in complex geometries', *J. Non-Newtonian Fluid Mech.*, **24**, 85–96 (1987).
8. P. W. Yeh, 'Finite element simulation of viscoelastic fluid flow through a sudden contraction', *Ph.D. Thesis*, Massachusetts Institute of Technology, Cambridge, MA 1984.
9. S. A. White, A. D. Gotsis and D. G. Baird, 'Review of the entry flow problem: experimental and numerical', *J. Non-Newtonian Fluid Mech.*, **24**, 121–160 (1987).
10. M. J. Crochet, A. R. Davies and K. Walters, *Numerical Simulation of Non-Newtonian Flow*, Elsevier, Amsterdam, 1984.
11. A. N. Beris, R. C. Armstrong and R. A. Brown, 'Perturbation theory for viscoelastic fluids between eccentric rotating cylinders', *J. Non-Newtonian Fluid Mech.*, **13**, 109–148 (1983).
12. A. N. Beris, R. C. Armstrong and R. A. Brown, 'Spectral/finite-element calculations of the flow of a Maxwell fluid between eccentric rotating cylinders', *J. Non-Newtonian Fluid Mech.*, **22**, 129–167 (1987).
13. R. C. King, M. R. Apelian, R. C. Armstrong and R. A. Brown, 'Numerically stable finite element techniques for viscoelastic calculations in smooth and singular geometries', *J. Non-Newtonian Fluid Mech.*, **29**, 147–216 (1988).
14. B. Debbaut, J. M. Marchal and M. J. Crochet, 'Numerical simulation of highly viscoelastic flows through an abrupt contraction', *J. Non-Newtonian Fluid Mech.*, **29**, 119–146 (1988).
15. A. I. Leonov, 'Non-equilibrium thermodynamics and rheology of viscoelastic polymer media', *Rheol. Acta*, **15**, 85–98 (1976).
16. A. I. Leonov, E. H. Lipkina, E. D. Paskhin and A. N. Prokunin, 'Theoretical and experimental investigation of shearing in elastic polymer liquids', *Rheol. Acta*, **15**, 411–426 (1976).
17. A. I. Isayev and C. A. Hieber, 'Oscillatory shear flow of polymeric systems', *J. Polym. Sci., Polym. Phys. Ed.*, **20**, 423–440 (1982).

18. R. K. Upadhyay, A. I. Isayev and S. F. Shen, 'Transient shear flow behavior of polymeric fluids according to the Leonov model', *Rheol. Acta*, **20**, 443–457 (1981).
19. A. I. Isayev and C. A. Hieber, 'Toward a viscoelastic modelling of the injection molding of polymers', *Rheol. Acta*, **19**, 168–182 (1980).
20. R. K. Upadhyay and A. I. Isayev, 'Simulation of two-dimensional planar flow of a viscoelastic fluid', *Rheol. Acta*, **25**, 80–94 (1986).
21. M. Viryayuthakorn and B. Caswell, 'Finite element simulation of viscoelastic flow', *J. Non-Newtonian Fluid Mech.*, **6**, 245–267 (1980).
22. A. Agrawal and P. R. Dawson, 'A comparison of Galerkin and streamline techniques for integrating strains from an Eulerian flow field', *Int. j. numer. methods eng.*, **21**, 853–881 (1985).
23. E. G. Thompson, J. F. T. Pittman and O. C. Zienkiewicz, 'Some integration techniques for the analysis of viscoelastic flows', *Int. j. numer. methods fluids*, **3**, 165–177 (1983).
24. L. G. Leal, M. M. Denn and R. Keunings, 'Lake Arrowhead Workshop Special Issue Papers—Introduction', *J. Non-Newtonian Fluid Mech.*, **29**, 1–8 (1988).
25. G.-G. Lin, H.-C. Tseng and Y.-H. Ju, 'Finite element technique to solve the elastic strain for Leonov fluid flow', *Int. j. numer. methods fluids*, **9**, 1059–1072 (1989).
26. C. D. Han and L. H. Drexler, 'Studies of converging flows of viscoelastic polymeric melts. III. Stress and velocity distributions in the entrance region of a tapered slit die', J. Appl. Polym. Sci., **17**, 2369–2393 (1973).
27. R. K. Upadhyay, 'Simulation of viscoelastic flows at large deformations according to the Leonov model', *Ph.D. Thesis*, Cornell University, Ithaca, NY, 1982.
28. C. D. Han, 'Wall normal stresses and die swell behavior of viscoelastic polymeric melts in flow through converging ducts', *AIChE J.*, **19**, 649–651 (1973).